Received: 30 November 2023 | Revised: 14 April 2024 | Accepted: 17 June 2024

DOI: 10.1002/jbio.202300505

RESEARCH ARTICLE

JOURNAL OF BIOPHOTONICS

Ultrabroadband two-beam coherent anti-Stokes Raman scattering and spontaneous Raman spectroscopy of organic fluids: A comparative study

Timea Koch[1] | **Roland Ackermann**[1] | **Axel Stoecker**[2] | **Tobias Meyer-Zedler**[3,4] | **Thomas Gabler**[1] | **Tom Lippoldt**[1] | **Jeannine Missbach-Guentner**[5] | **Christoph Russmann**[2,5] | **Jürgen Popp**[4] | **Stefan Nolte**[1,6]

[1]Institute of Applied Physics, Abbe Center of Photonics, Friedrich-Schiller-Universität Jena, Jena, Germany

[2]Faculty of Engineering and Health, University of Applied Science and Arts, Goettingen, Germany

[3]Institute of Physical Chemistry and Abbe Center of Photonics, Friedrich-Schiller-Universität Jena, Jena, Germany

[4]Leibniz Institute of Photonic Technology, Jena, Germany

[5]Department of Diagnostic and Interventional Radiology, University Medical Center, Goettingen, Germany

[6]Fraunhofer Institute for Applied Optics and Precision Engineering IOF, Jena, Germany

Correspondence
Roland Ackermann, Institute of Applied Physics, Abbe Center of Photonics, Friedrich-Schiller-Universität Jena, D-07745 Jena, Germany.
Email: roland.ackermann@uni-jena.de

Funding information
Deutsche Forschungsgemeinschaft, Grant/Award Number: 428490203; European Union's Horizon 2020 research and innovation program, Grant/Award Number: 101016923

Abstract

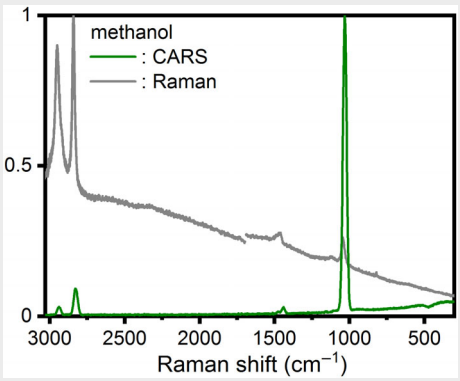

Spontaneous Raman spectroscopy is a well-established diagnostic tool, allowing for the identification of all Raman active species with a single measurement. Yet, it may suffer from low-signal intensity and fluorescent background. In contrast, coherent anti-Stokes Raman scattering (CARS) offers laser-like signals, but the traditional approach lacks the multiplex capability of spontaneous Raman spectroscopy. We present an ultrabroadband CARS setup which aims at exciting the full spectrum (300–3700 cm^{-1}) of biological molecules. A dual-output optical parametric amplifier provides a ∼7 fs pump/Stokes and a ∼700 fs probe pulse. CARS spectra of DMSO, ethanol, and methanol show great agreement with spontaneous Raman spectroscopy and superiority in fluorescent environments. The spectral resolution proves sufficient to differentiate between the complex spectra of L-proline and hydroxyproline. Moreover, decay constants in the sub picosecond range are determined for individual Raman transitions, providing an additional approach for sample characterization.

KEYWORDS

coherent anti-Stokes Raman spectroscopy, organic fluids, Raman microscopy, Raman spectroscopy, ultrabroadband CARS, ultrashort laser pulse, vibrational spectroscopy

1 | INTRODUCTION

Spontaneous Raman spectroscopy (SpRS) is a versatile diagnostic tool in various fields, ranging from microscopic medical applications to industrial combustion research [1]. Its multiplex capability allows identifying all Raman active species by the acquisition of a single spectrum, and potentially, the determination of species concentration and temperature. However, Raman scattering cross-sections are typically small, requiring high laser powers and/or long acquisition times, which in turn may lead to sample damage or other alteration. In tissue diagnostics, Raman lines may moreover be masked by fluorescence [2, 3].

Higher intensities and laser-like signals are provided by coherent Raman scattering (CRS), that is, stimulated (SRS), coherent Stokes (CSRS), and coherent anti-Stokes Raman scattering (CARS). The original three-beam CARS schemes require a proper choice of the laser wavelengths, as only specific Raman transitions matching the wavelength difference between pump and Stokes pulse are probed. Hence, the multiplex feature of SpRS is lost. (Ultra-)Broadband CARS approaches address this issue by providing pulses with sufficient bandwidth to cover Raman transitions of multiple species [4]. In a pioneering work, Dudovich et al. used a single beam scheme and a spatial light modulator (SLM) for coherent control Raman spectroscopy in simple liquids [5]. Subsequent studies have focused on both selective molecular excitation by pulse shaping techniques [6–8] as well as on reliable CARS implementations. Regarding the latter, most of the investigations have addressed selected spectral windows. Excitation of the fingerprint region (<1500 cm^{-1}) is possible with moderately short pulses (10–15 fs), which can be generated, for example, by ~40 fs seed pulses from a standard Ti:sapphire regenerative amplifier [9]. Further spectral broadening is optionally induced by downstream nonlinear components such as crystals or optical fibers. Numerous studies relied on this configuration for CARS experiments on liquids and biological tissue. Prince et al. acquired Raman spectra of Rhodamine 6G in methanol, toluene, and chloroform up to shifts of ~1700 cm^{-1} [10]. Plewicki and Levis identified Raman signals of methanol and acetone at ~3000 cm^{-1} [11]. The Raman decay of the CH-stretching modes of methanol and ethanol was determined in a BOXCARS configuration [12–14].

Recent advances focus on replacing the Ti:sapphire seed lasers by more robust systems such as fiber lasers. Single shot detection of bacterial spores has been shown with this approach [15]. Camp et al. report on the excitation of the fingerprint region and the typical CH stretching modes (~3000 cm^{-1}), using a broadband 16 fs pump pulse and a narrowband 3.4 ps probe pulse at 770 nm from a fiber laser [16]. However, Raman excitation is different for both spectral regions. For the fingerprint region, Raman excitation is performed by the 16 fs pulse itself, whereas transitions with larger shifts are excited by both the broadband pulse and the narrowband pulse, which acts as pump and probe pulse in this case. The Raman shifts from 600 to 3600 cm^{-1} have been addressed using a Nd:YVO_4 microchip laser and a photonic crystal fiber for spectral broadening, using the maximum entropy method to remove the nonresonant background [17, 18]. In a very recent study, Vernuccio et al. have used a sub 20 fs Stokes pulse and a narrowband pump pulse to generate Raman like spectra in the range of 400–3100 cm^{-1} [19]. The nonresonant background was removed via a time-domain Kramers–Kronig algorithm.

In the present study, we aim at exciting Raman transitions up to 3700 cm^{-1} using a sub 10 fs pulse to generate SpRS-like CARS spectra, which are easily interpretable without postprocessing. For this purpose, we implement an ultrabroadband two-beam CARS setup using the sub 10 fs pulse as pump and Stokes and a narrowband pulse as probe at 517 nm. A time delay between the Raman excitation from the pump/Stokes pulse and the probe pulse is implemented to avoid nonresonant background and minimized to avoid bias from different Raman dephasing times of the peaks involved. The used laser system is a dual output optical parametric chirped-pulse amplifier (OPCPA). This laser system was originally designed for gas analysis in combustion and gasification research. In particular, the system allows for the detection of H_2 with a Raman shift of ~4160 cm^{-1} [20]. Therefore, both the typical CH stretching modes (~3000 cm^{-1}) and the region below 1500 cm^{-1} as well as liquid water (3000–3700 cm^{-1}) are easily covered by the pump/Stokes spectrum [21]. Tailored spectral resolution is provided by the probe pulses adjustable spectral width. To prove the functionality and advantages of the newly implemented system, the results of the CARS measurements are compared with SpRS.

2 | EXPERIMENTAL SETUP

2.1 | CARS measurements

The scheme of the CARS setup is shown in Figure 1. The ~7 fs pump/Stokes pulse and the narrowband probe pulse are provided by a commercial dual output OPCPA laser system with a repetition rate of 200 kHz (venteon OPCPA, Laser Quantum GmbH, Konstanz, Germany). The maximum specified pulse energy is $E_{pump/Stokes} = 10$ μJ for the ~7 fs pulse (700–1000 nm 25 dB bandwidth) and $E_{probe} = 20$ μJ for the probe pulse at 517 nm. The pulse duration of the probe pulse, measured with a commercial

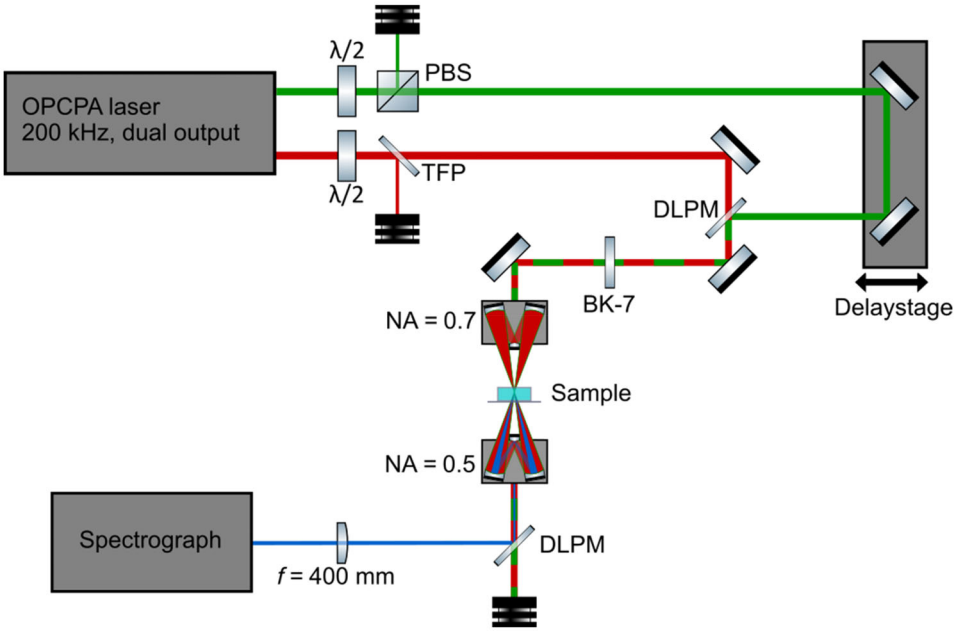

FIGURE 1 Scheme of the two-beam ultrabroadband coherent anti-Stokes Raman scattering setup. An ultrabroadband, near-infrared 7 fs beam (red) and a 678 fs beam at 517 nm (green) are provided by a 200 kHz optical parametric chirped-pulse amplifier (OPCPA). PBS, polarizing beam splitter; TFP, thin-film polarizer; DLPM, dichroic long-pass mirror.

autocorrelator (pulseCheck, APE Angewandte Physik & Elektronik GmbH, Berlin, Germany), is adjustable by a variable slit in the compressor of the OPCPA. In the presented study, we choose a probe pulse duration of 678 fs, as it is the shortest possible in the current system configuration and should on one hand provide sufficient spectral resolution but should also allow for probing the quickly decaying (∼0.1–1 ps) impulsive Raman excitation. The corresponding spectral width of the probe is 0.67 nm or 25 cm^{-1} at full width half maximum (FWHM). The compressor of the pump/Stokes pulse consists of chirped mirrors and an adjustable wedge pair for fine tuning. It was designed for previous experiments in which the dispersion induced by windows of a gas cell should be compensated. For the current experiment, chirp optimization is achieved by maximizing the CARS signal at ∼3000 cm^{-1} in ethanol by inserting 5 mm of BK-7 into the beam path and fine-tuning of the compressor wedges. The pulse duration of the pump/Stokes pulse is characterized by a Michelson interferometer-based autocorrelator (Femtometer, mks Spectra-Physics, Santa Clara, USA).

The two beams are spatially overlapped using a thin dichroic long-pass mirror (DLPM, DMLP550-∅1, Thorlabs, Bergkirchen, Germany). Temporal overlap is controlled by an automated delay stage with a minimum temporal step size of 33 fs (M-414.1PD, Physik Instrumente (PI) GmbH & Co. KG, Karlsruhe, Germany). For each sample, the delay t_d at which the pump/Stokes and the probe pulse temporally overlap is determined by a separate delay scan with reduced signal intensity to avoid saturation in a nonresonant spectral range (230–310 cm^{-1}). Then, $t_d = 0$ is defined by the spectrum with maximum integrated intensity in this spectral range. Thereafter, the laser pulse energies are increased to maximize the signal intensity at $t_d \approx 470$ fs for each sample individually. Typical pulse energies at the sample position are 151–216 nJ for the pump/Stokes pulse and 15–133 nJ for the probe pulse. The energy adjustments are made by a half-wave plate with a downstream thin film polarizer (TFP) for the ∼7 fs pulse and a polarizing beam splitter (PBS) for the probe pulse, respectively.

CARS signal generation involving sub 10 fs pulses in a collinear configuration must consider both the effect of dispersion and efficient phase-matching. The latter is provided by sufficiently high numerical apertures (NAs) [22], whereas dispersion is avoided by reflective optics. The beam is therefore focused by a reflective Schwarzschild type objective with a NA of 0.7 (891-0001, Pike Technologies, Madison, USA). Assuming a Gaussian beam at a central wavelength of 800 nm yields a theoretical focus radius of $r_{focus} = 0.36$ µm. A second reflective objective (NA = 0.5, 25-0522, Ealing Electro-Optics plc, Watford, UK) is used for light collection. It is mounted on a manual x-y-z-translation stage to match the collimation of the CARS signal to the refractive index of the different samples. The custom-made sample holder and the reflective objectives are vertically orientated with respect to the optical table. A sample volume of ∼1.2 mL is sealed with a 3.9 mm high metal ring between two 100 µm thin cover glasses. The residual pump/Stokes and pump beams are each removed by two dichroic long pass mirrors (DMLP650 and DMLP505, Thorlabs, Bergkirchen, Germany). The reflectance edge (∼50% at 509 nm) of the latter defines the smallest Raman shift of the setup we included in our study, which is 300 cm^{-1}. The CARS signal is focused into a spectrograph (Shamrock 500i with

Newton DU940P-BU2 CCD, Andor Technology, Belfast, Ireland) using a 400 mm cylindric lens (LJ1363L1-A, Thorlabs, Bergkirchen, Germany). In this experiment, we use the internal 600 L/mm (blaze 500 nm) grating of the spectrometer providing a spectral range of ~4000 cm^{-1} and a resolution of 0.043 nm. The camera provides a resolution of 2048 × 512 pixels and is used in full vertical binning (FVB) mode, for which the shortest provided acquisition time is 4.5 ms. Therefore, a minimum of ~1000 pulses may be recorded. In this case, the exposure is almost entirely governed by the (overclocked) vertical pixel shift speed (7.3 µs/row ≙ 3.7 ms) and readout time (f_{pixel} = 3 MHz ≙ 0.6 ms) of the CCD sensor. As this renders some uncertainty about the actual number of pulses, which are acquired, the shortest possible exposure time is only used to test the performance limit of the setup. Otherwise, the exposure time is set to 50 ms, and 10 spectra are accumulated. From each CARS spectrum, a dark image is then subtracted.

Our focus is on testing a fast and simple measurement method to create SpRS like CARS signals excluding post-processing. An algorithm-based approach would require a measurement of the pure nonresonant background, which can be made in noble gases such as argon. However, our setup only allows for measurements in liquids and transparent solids, which show more complex behaviors. The recording of a pure nonresonant background in those samples needs careful consideration. To achieve a straight-forward measurement method instead, we choose the approach of a pulse delay to remove the nonresonant background over an algorithm-based process. Because of the delay, peak intensities are expected to decrease according to their individual Raman dephasing times, which will be discussed in the section "Time resolved CARS" below. A further intensity correction was not performed as peaks across the entire spectrum are sufficiently high to identify species, which is the goal of the setup. For quantitative analysis, however, our previous investigations have shown that spectral referencing in argon would be necessary especially for Raman shifts ≥3000 cm^{-1} [20, 23], which was not possible in this setup for previously mentioned reasons. We expect a signal intensity decrease with increasing Raman shift due to the factors explained in the following. Over the recorded spectral range of 425–513 nm, the grating efficiency increases from ~60% to ~75%, whereas the CCD sensor efficiency remains at ~65%. Additionally, the excitation efficiency in ultrabroadband two-beam CARS is reduced for higher Raman shifts due to less matching wavelength pairs within the spectrum. The used pump/Stokes spectrum furthermore shows an uneven intensity decline with rising wavelength as can be seen in Figure 2A, where it is displayed for three different CARS measurements. The delay of the pump and the seed pulse in the second amplifier of the OPCPA can be adjusted to find a compromise between a smooth spectral intensity profile and maximum spectral width. The corresponding autocorrelation trace is shown in Figure 2B and yields a pulse duration of 7.3 fs for the pump/Stokes pulse.

2.2 | SpRS measurements

SpRS measurements are conducted using a commercial Raman microscope (inVia Raman microscope, Renishaw plc, Wotton-under-Edge, UK). We use an excitation wavelength of 473 nm, which is close to the observed CARS signals (300–3700 cm^{-1} ≙ 434–509 nm), and a 5× focusing objective. Raman signals are detected in reflection mode with the same objective and a subsequent spectrometer with a 2400 L/mm grating. The same sample holder as with the CARS measurements is used. To cover Raman shifts up to ~3700 cm^{-1}, four spectra for different grating positions are assembled. The acquisition time for

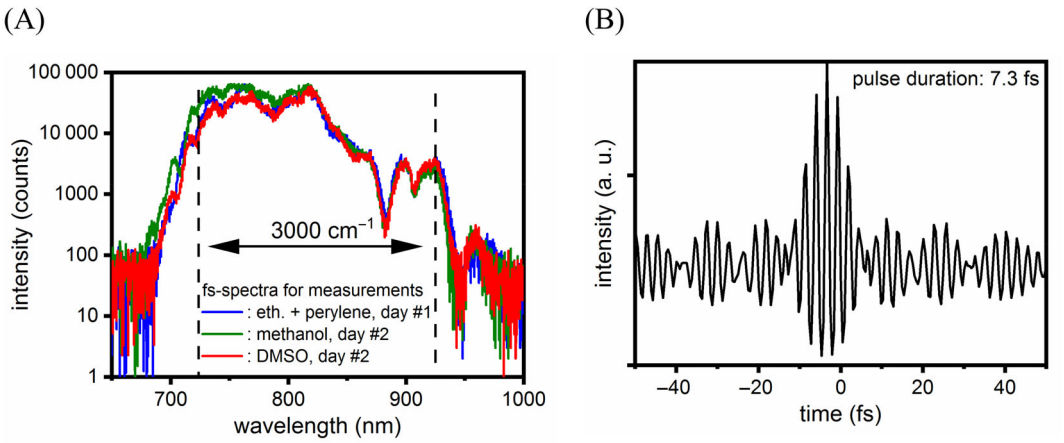

FIGURE 2 (A) Three spectra of the sub 10 fs pulse and (B) an autocorrelation trace. DMSO, dimethyl sulfoxide.

all (cw-)Raman measurements is set to 1 s with 10 spectra accumulated, therefore, having an 80 times longer total acquisition time for the entire spectral range than in the CARS measurements. For each SpRS measurement, a spectrum without sample but laser on is subtracted. A further correction for the spectrometer efficiency using a calibrated light source is not performed, as the spectral window of the detected Raman signals is relatively small (480–551 nm), and a precise determination of the intensity ratios is beyond the scope of this study.

2.3 | Samples

To test the functionality of the setup, we use dimethyl sulfoxide (DMSO, 99.9%, Runika e.K., Viernheim, Germany), methanol (≥99.5%, Carl Roth GmbH + Co. KG, Karlsruhe, Germany), and ethanol (≥ 99%, Fisher Scientific GmbH, Schwerte, Germany). To further test the effects of fluorescence, perylene (≥98%, Fisher Scientific GmbH) is mixed into ethanol in a concentration of 50 µg/g. The absorption of perylene ranges from <200 nm to slightly above the excitation wavelength of 473 nm used in the Raman microscope. It emits light at 436–465 nm, where the Raman signal of both methods is supposed to be. Lastly, L-proline (H-Pro-OH, BLD Pharmatech GmbH, Reinbek, Germany) and hydroxyproline ((2S,4R)-4-hydroxypyrrolidine-2-carboxylic acid, BLD Pharmatech GmbH, Reinbek, Germany) are dissolved in water at 25% and used to test the detectability of more complex molecular structures.

3 | RESULTS AND DISCUSSION

3.1 | Comparison of CARS and SpRS spectra for simple organic fluids

Figure 3A shows the CARS spectra in DMSO for three different probe pulse delays with pulse energies at the sample position of $E_{\text{pump/Stokes}} = 194$ nJ and $E_{\text{probe}} = 67$ nJ. At $t_d = 0$, the CARS spectrum shows

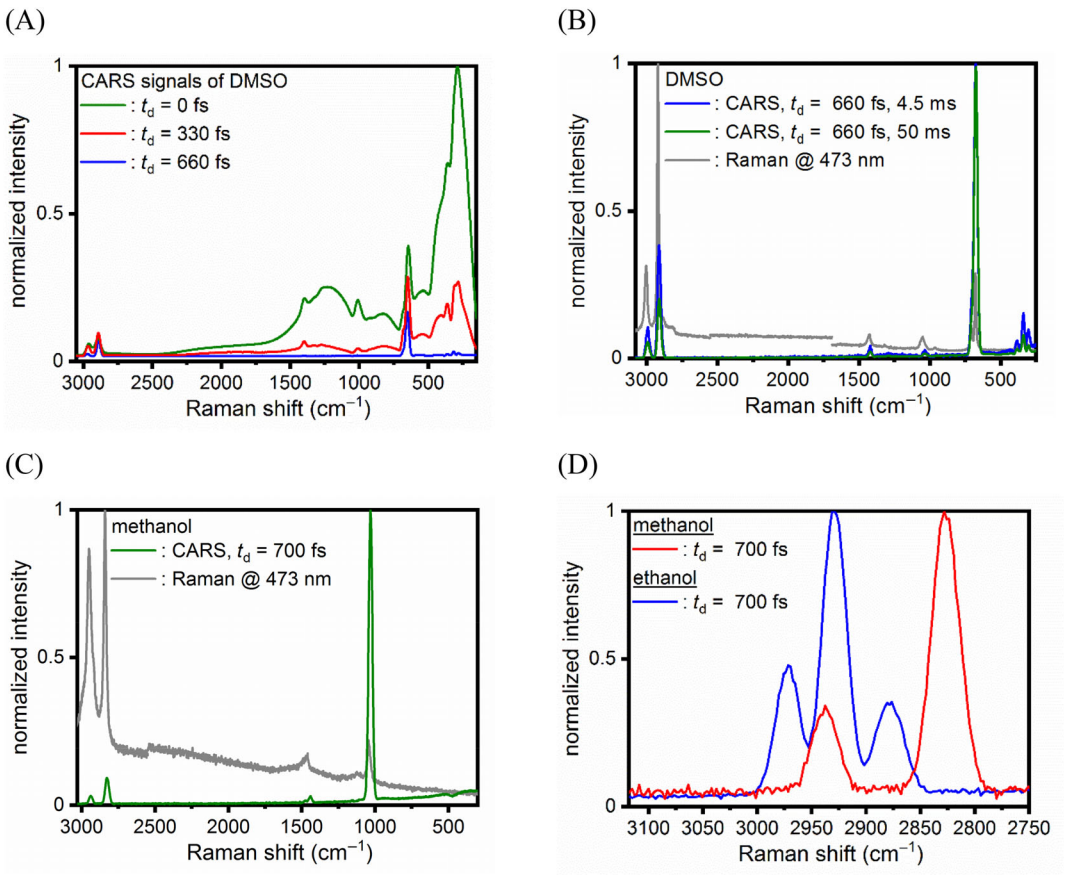

FIGURE 3 (A) Coherent anti-Stokes Raman scattering (CARS) spectra for dimethyl sulfoxide (DMSO) at different probe delays. The spectra are normalized to the largest peak for $t_d = 0$ fs. (B) Comparison of spontaneous Raman spectroscopy (grey line) with CARS spectra at 50 ms with 10 accumulations (green line) and 4.5 ms with one accumulation (blue line) for DMSO and (C) methanol. (D) CARS spectra for methanol (red line) and ethanol (blue line) at ~2900 cm^{-1}. Spectra in (B–D) are normalized to the largest peak of each spectrum.

considerable, but nonuniform nonresonant contribution. For small shifts (<500 cm^{-1}), resonant spectral features like the characteristic three-way comb are completely masked by the nonresonant background, which is decreasing quickly for larger probe pulse delays ($t_d = 330$ fs, Figure 3A, red line) and completely vanishes at $t_d = 660$ fs. The dephasing comes along with an individual intensity decrease for each resonant peak. While the peaks at 2910 and 674 cm^{-1} remain mostly unchanged, the peaks at 2993, 1421, and 1034 cm^{-1} are visibly reduced yet clearly identifiable. Comparing SpRS and CARS spectra at $t_d = 700$ fs (Figure 3B), the same spectral features are observed. The major peaks of DMSO can be found at 2993 and 2910 cm^{-1}, characteristic for the CH stretch and 674 cm^{-1} signing the CS stretch. Further smaller peaks are assigned to the CH deformation (1421 cm^{-1}), the SO stretch (1034 cm^{-1}), and the CSO rock and CSC bend (300–400 cm^{-1}) [24]. All features of DMSO appear with a high signal-to-noise ratio even with the shortest available acquisition time of 4.5 ms (blue line). Figure 3C shows the CARS and SpRS spectra for methanol ($E_{pump/Stokes} = 151$ nJ, $E_{probe} = 15$ nJ, $t_d = 700$ fs). As the chemical structures of DMSO and methanol share some similarities, the CARS and SpRS spectra of both samples show peaks in the same areas. The CH stretching generates Raman lines at 2937 and 2828 cm^{-1}, the CH deformation leads to a peak at 1438 cm^{-1}, and at 1029 cm^{-1} the CO stretch can be found [21]. CARS spectra in both liquids are quasi background free over the whole range from 300 to 3700 cm^{-1}. Because of previously explained reasons, the peak intensities at 3000 cm^{-1} are always considerably lower than at ~1000 cm^{-1} for CARS. This is opposite to our SpRS spectra, which are, however, not corrected for spectrometer efficiency, and to spectra found in SpectraBase, where an intensity ratio of I_{2840}:$I_{1036} \sim 0.65$:1 for methanol and I_{2910}:$I_{674} \sim$ 1:0.65 DMSO is reported [25].

Despite the reduced signal intensity at ~3000 cm^{-1}, Raman peaks are sufficiently high to be used as characterization feature. This is proven when we compare the Raman spectra of methanol and ethanol for the CH stretching region. The pulse energies for the ethanol measurement were set to the same values as for methanol, and the delay was set to $t_d = 700$ fs. The similarly structured liquids can easily be differentiated by their Raman lines, as can be seen in Figure 3D. While methanol produces two lines at 2828 and 2937 cm^{-1}, ethanol can be identified by three characteristic peaks at 2878, 2929, and 2971 cm^{-1} [26, 27]. Additionally, no nonresonant background occurs for high Raman shifts, giving the opportunity to use spectra of lower time delays and thus increasing the CARS signal intensity to identify species.

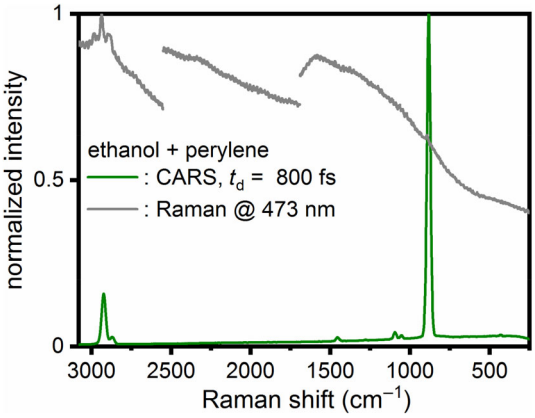

FIGURE 4 Comparison of spectrum from spontaneous Raman spectroscopy (grey line) with coherent anti-Stokes Raman scattering (CARS) spectrum for ethanol with perylene.

Besides the nonresonant-background, other effects like fluorescence might negatively impact measurements. To evaluate the effect of fluorescence, the fluorescence marker perylene was mixed into ethanol. Figure 4 shows the SpRS and CARS ($E_{pump/Stokes} = 194$ nJ, $E_{probe} = 15$ nJ) spectra of this sample. The CARS spectrum ($t_d = 800$ fs) is roughly unaffected by the fluorescent dye, whereas the Raman peaks <3000 cm^{-1} are completely overshadowed by fluorescence for SpRS, only the strong peak at 889 cm^{-1} is barely identifiable. As with previous measurements, the peak intensity declines for higher Raman shifts. The concentration of perylene itself is too low to be detected by CARS or SpRS, respectively.

3.2 | Comparison of CARS and SpRS spectra for amino acids

Lastly, the CARS spectra of the amino acids L-proline and hydroxyproline are investigated. Figure 5 displays their fluorescence-impacted Raman (grey) and fluorescence-free CARS (red, blue) spectra covering 300–3000 cm^{-1} and visualizing the improvement of the CARS spectra with averaging. For both acids, two CARS measurements with 10 accumulations (blue line) and 100 accumulations (red line) are normalized and compared, proving high reproducibility and good signal to noise ratio of the acquired spectra. Figure 6 displays a zoomed in image of the CARS spectra of L-proline (blue line) and hydroxyproline (green line) at 2750–3750 cm^{-1}. The pulse energy in the CARS setup is $E_{pump/Stokes} = 216$ nJ and $E_{probe} = 133$ nJ.

The SpRS spectra show distinctive peaks in the 3000 cm^{-1} region. However, most of the bands at 500–1600 cm^{-1} can hardly be identified due to the low signal-to-noise ratio and high autofluorescence

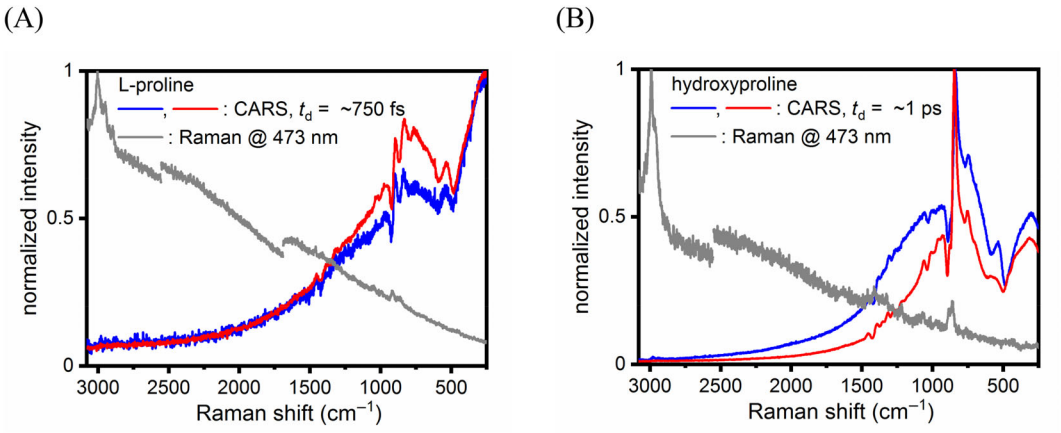

FIGURE 5 Coherent anti-Stokes Raman scattering (CARS) spectra for two measurements, one with 10 accumulations (blue line) and one with 100 accumulations (red line), as well as SpRS spectra for (A) L-proline and (B) hydroxyproline.

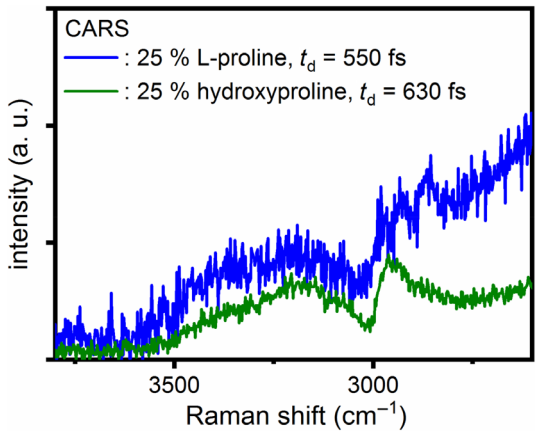

FIGURE 6 Coherent anti-Stokes Raman scattering (CARS) spectra for L-proline and hydroxyproline at a Raman shift of 2750–3750 cm^{-1}.

background, which increases with Raman shift. Therefore, the SpRS spectra acquired in this study are not used as reference for the CARS spectra. Instead, we use literature values. Zhu et al. collected Raman spectra of L-proline in aqueous solution at 3 g/100 mL using a Renishaw HPNIR Raman spectrometer with a 20× objective and an acquisition time of 10 s [28]. Other than in the here presented study, the excitation wavelength was set to 785 nm, most likely avoiding fluorescence.

As with the perylene/ethanol mixture, the CARS setup successfully discriminates against fluorescence, providing clear spectra. The CARS spectra of both amino acids show high numbers of Raman bands in the fingerprint region of 500–1600 cm^{-1}, characteristic for, for example, the CH_2 rocking and twisting mode, while the symmetric and asymmetric CH_2 stretch are observed at 2900–3000 cm^{-1} [29]. The three peaks at high Raman shifts (~3000 cm^{-1}), the characteristic band at 1452 cm^{-1} signing the CH_2 bending vibration and the skeletal stretching vibration at ~840 cm^{-1} help to identify L-proline [28]. The high intensity peak at 844 cm^{-1} assigned to the CH_2 twisting is characteristic for hydroxyproline [30, 31]. Other than in the measurements on simple liquids, peaks appear wider and with lower intensity while suffering a higher background. In consequence, some typical Raman bands cannot be identified. Peak intensities generally tend to be lower for amino acids compared with simple structured molecules like ethanol and methanol, as can be seen in the literature [32]. However, most papers investigated solid samples of high concentration. Unlike that the here presented CARS setup works in transmission mode, only allowing measurements of transparent solutions with reduced concentrations. Another downside of working with solutions is the broadening of Raman lines [28]. This effect adds to the medium spectral resolution due to the probe pulse width, which as a compromise for time resolution was set to a FWHM of ~0.67 nm (≙25 cm^{-1}) in this study. This value is close to the Fourier transform limit (0.58 nm ≙ 22 cm^{-1}) for the probe pulse duration determined by autocorrelation (678 fs). Consequently, closely lying Raman peaks at low Raman shifts may overlap leading to increased background. As with previous studies on gas analysis (t_{probe} = 1.6 ps) [20], the slit size in the OPCPA compressor can be matched to the necessary spectral resolution if temporal resolution does not play a role. Nevertheless, two independent measurements (red and blue lines in Figure 5A,B) show that the observed spectral features are specific to the corresponding amino acid. As expected, 10 accumulations (blue line) show higher noise than 100 accumulations (red line), but with reproducible spectral features. As discussed above, the spectrum of the pump/Stokes pulse shows high shot-to-shot stability [23]. We therefore attribute the

fluctuations in signal intensity for Raman shifts <1500 cm^{-1} to sample alterations such as heating.

Figure 6 additionally reveals the broadband CARS signal of liquid water at 3000–3700 cm^{-1}, which is an indication that the solutions are still in the liquid phase, as water vapor would show a discrete Raman shift at 3657 cm^{-1} [33]. This is remarkable, as the breakdown threshold for ultrashort pulses in water is ~1 J/cm^{-2} (100 fs) [34], which we surpass significantly in this study (36–52 J/cm^2 for $r_{focus} = 0.36$ µm). Possible reasons for the observation of the liquid phase are a spatial and temporal pulse degradation during its propagation through the sample. We indeed observe a crucial dependence of the CARS signal strength on the vertical focus position within the sample. The same holds for adjustments of the chirp using the compressor wedges. Furthermore, pulse propagation through a Schwarzschild type objective needs careful alignment to avoid obstructions from the objective mirrors. Based on these proof-of-principle investigations, we are therefore planning a systematic study on different NAs, which compares the effect of Schwarzschild type objectives and off-axis parabolic mirrors on the focus quality and the resulting CARS signal. Furthermore, we also consider reflective signal detection, which on one hand reduces signal strengths for transparent samples, but also avoids pulse degradation caused by the transmission through the sample and opens path for investigations on nontransparent samples.

3.3 | Time resolved CARS

The CARS setup offers the option to investigate the time dependence of individual Raman lines and nonresonant background and thus to measure the Raman decay time. For this purpose, we delayed the probe pulse in steps of 33 fs. Pulse energies remained as previously mentioned for DMSO and methanol.

Figure 7A shows the time dependence of the nonresonant signal during DMSO and methanol measurements. The nonresonant signal exhibits a symmetric shape and drops by ~2 orders of magnitude at $t_d \sim 500$ fs. Exemplarily, a Gaussian fit yields a FWHM of 650 fs for the DMSO measurement, which is in good agreement with the abovementioned probe pulse duration determined by autocorrelation (678 fs).

In Figure 7B, the time dependence of the C—H degenerate stretch (2993 cm^{-1}), C—H symmetric stretch (2910 cm^{-1}), and C—S symmetric stretch (674 cm^{-1}) of DMSO are displayed [35]. Exponential fits and normalization refer to $t_d = 700$ fs to avoid interference from the nonresonant background. The peak intensity decrease follows a simple exponential decay with decay constants of $T_{2993} = 0.24 \pm 0.02$ ps, $T_{2910} = 0.62 \pm 0.08$ ps, and $T_{674} = 0.57 \pm 0.05$ ps, respectively. To our knowledge, this is the first determination of the Raman decay due to dephasing of the vibrational coherence in pure DMSO. The different decay times are roughly confirmed by the widths of the SpRS signals. Assuming a Voigt profile, the FWHM is 21 cm^{-1} for the peak at 2993 and 12 cm^{-1} for the peak at 2910 cm^{-1}, which yield decay times of $T_{SpRS,2993} \sim 0.25$ ps and $T_{SpRS,2910} \sim 0.44$ ps. Martens et al. report a similar width ratio, but smaller absolute widths of these SpRS signals (9.4 vs. 5.4 cm^{-1}) at 298 K and identified underlying peaks at 77 K [24]. However, a further discussion of this behavior is beyond the scope of this study. Zhao et al. determined comparable decays for the three peaks at ~3000 cm^{-1} in ethanol ($T_{2973} = 0.284$ ps, $T_{2927} = 0.771$ ps, $T_{2878} = 0.556$ ps) [12]. Such additional information about the Raman decay may help to identify

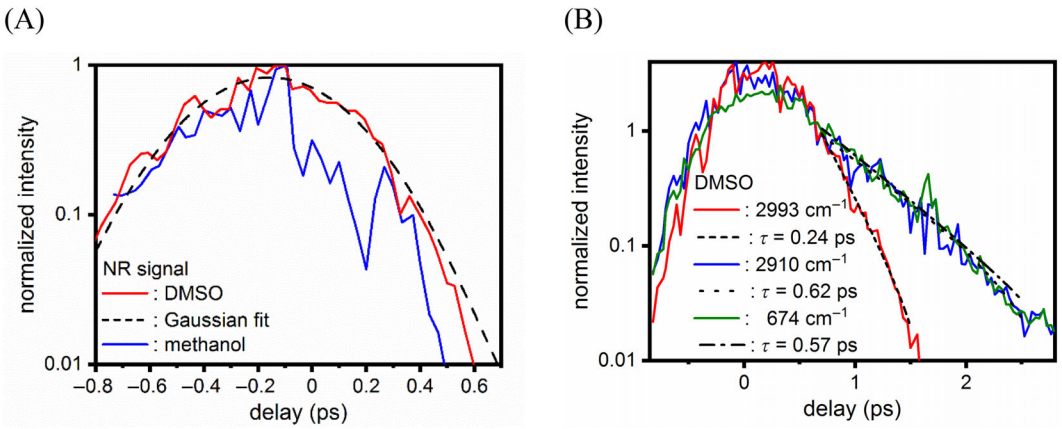

FIGURE 7 (A) Time dependence of the nonresonant signal for the dimethyl sulfoxide (DMSO) (with Gaussian fit) and methanol measurements (Figure 2). The FWHM of the Gaussian fit is 650 fs. (B) Raman decay of three different Raman lines of DMSO and corresponding fits for a simple exponential decay.

and differentiate between species and individual peaks in a straightforward fashion.

4 | CONCLUSION

In this study, we present an ultrabroadband two-beam CARS setup. With this approach, Raman shifts up to ~3700 cm^{-1} have been observed with sufficient spectral resolution to differentiate between complex structures, while also providing decay information about individual Raman lines.

The setup uses a dual output OPCPA providing a 7 fs broadband pump/Stokes pulse at ~800 nm and a 700 fs probe pulse at 517 nm, tuneable in its spectral width and time resolution. A delay stage was used for a time delay between the two pulses to avoid nonresonant background and investigate the time dependence of individual Raman lines.

The acquired CARS spectra of DMSO, methanol, and ethanol are in good agreement with literature and SpRS spectra. They could be easily interpreted without further postprocessing being quasi free of any background or fluorescence when mixed with perylene. CARS spectra had sufficient spectral resolution to differentiate L-proline from hydroxyproline both in the CH stretching region (~3000 cm^{-1}) as well as the fingerprint region (<1500 cm^{-1}). In exchange for spectral resolution, the probe pulse duration and by that the nonresonant background were minimized to ~650 fs allowing for investigating sub picosecond decay constants. Three exemplarily chosen DMSO Raman lines were determined to have decay constants of $T_{2993} = 0.24$ ps, $T_{2910} = 0.62$ ps, and $T_{674} = 0.57$ ps.

CARS spectra with a minimum acquisition time of 4.5 ms (~1000 pulses), currently limited by the CCD camera of the spectrometer, have been recorded with sufficient signal-to-noise ratio. This allows for the future implementation of a scanning system, for example, for tissue imaging. Further efforts on the setup will on one hand focus on switching to reflection mode to investigate nontransparent samples. On the other hand, possible applications include rapid analysis of endogenous or exogenous fluids. The high available pulse energies allow also for mixed applications such as breath analysis, or an integrated system with tissue ablation and diagnosis ability [36].

ACKNOWLEDGMENTS

This study was funded by the Deutsche Forschungsgemeinschaft (DFG, German Research Foundation) - 428490203. T.M.Z. acknowledges funding from the European Union's Horizon 2020 research and innovation program under grant No 101016923. Open Access funding enabled and organized by Projekt DEAL.

CONFLICT OF INTEREST STATEMENT

The authors declare no financial or commercial conflict of interest.

DATA AVAILABILITY STATEMENT

The data that support the findings of this study are available from the corresponding author upon reasonable request.

ORCID

Roland Ackermann https://orcid.org/0000-0002-1239-4305

REFERENCES

[1] K. Kong, C. Kendall, N. Stone, I. Notingher, *Adv. Drug Delivery Rev.* **2015**, *89*, 121.
[2] D. A. Long, *The Raman Effect*, John Wiley & Sons Ltd., Chichester **2002**.
[3] C. Krafft, B. Dietzek, J. Popp, *Analyst* **2009**, *134*, 1046.
[4] D. Polli, V. Kumar, C. M. Valensise, M. Marangoni, G. Cerullo, *Laser Photonics Rev.* **2018**, *12*, 1800020.
[5] N. Dudovich, D. Oron, Y. Silberberg, *Nature* **2002**, *418*, 512.
[6] B. von Vacano, M. Motzkus, *Opt. Commun.* **2006**, *264*, 488.
[7] B. von Vacano, M. Motzkus, *Phys. Chem. Chem. Phys.* **2008**, *10*, 681.
[8] K. Isobe, A. Suda, M. Tanaka, H. Hashimoto, F. Kannari, H. Kawano, H. Mizuno, A. Miyawaki, K. Midorikawa, *Opt. Express* **2009**, *17*, 11259.
[9] N. Dudovich, D. Oron, Y. Silberberg, *J. Chem. Phys.* **2003**, *118*, 9208.
[10] B. D. Prince, A. Chakraborty, B. M. Prince, H. U. Stauffer, *J. Chem. Phys.* **2006**, *125*, 44502.
[11] M. Plewicki, R. Levis, *J. Opt. Soc. Am. B* **2008**, *25*, 1714.
[12] Y. Zhao, S. Zhang, B. Zhou, Z. Dong, D. Chen, Z. Zhang, Y. Xia, *Vib. Spectrosc.* **2014**, *73*, 24.
[13] Y. Zhao, S. Zhang, Z. Zhang, Z. Dong, D. Chen, Z. Zhang, Y. Xia, *Opt. Commun.* **2015**, *334*, 319.
[14] D. Pestov, M. Zhi, Z.-E. Sariyanni, N. G. Kalugin, A. Kolomenskii, R. Murawski, Y. V. Rostovtsev, V. A. Sautenkov, A. V. Sokolov, M. O. Scully, *J. Raman Spectrosc.* **2006**, *37*, 392.
[15] C. M. Valensise, A. Giuseppi, F. Vernuccio, A. De la Cadena, G. Cerullo, D. Polli, *APL Photonics* **2020**, *5*, 061305.
[16] C. H. Camp Jr., Y. J. Lee, J. M. Heddleston, C. M. Hartshorn, A. R. Hight Walker, J. N. Rich, J. D. Lathia, M. T. Cicerone, *Nat. Photonics* **2014**, *8*, 627.
[17] H. Kano, T. Maruyama, J. Kano, Y. Oka, D. Kaneta, T. Guerenne, P. Leproux, V. Couderc, M. Noguchi, *Opt. Continuum.* **2019**, *2*, 1693.
[18] H. Yoneyama, K. Sudo, P. Leproux, V. Couderc, A. Inoko, H. Kano, *APL Photonics* **2018**, *3*, 092408.
[19] F. Vernuccio, R. Vanna, C. Ceconello, A. Bresci, F. Manetti, S. Sorrentino, S. Ghislanzoni, F. Lambertucci, O. Motino, I. Martins, G. Kroemer, I. Bongarzone, G. Cerullo, D. Polli, *J. Phys. Chem. B* **2023**, *127*, 4733.

[20] Y. Ran, M. Junghanns, A. Boden, S. Nolte, A. Tünnermann, R. Ackermann, *J. Raman Spectrosc.* **2019**, *50*, 1268.
[21] A. Emin, A. Hushur, T. Mamtimin, *AIP Adv.* **2020**, *10*, 065330.
[22] A. Zumbusch, G. Holtom, X. Xie, *Phys. Rev. Lett.* **1999**, *82*, 4142.
[23] Y. Ran, A. Boden, A. Richter, S. Guhl, S. Nolte, R. Ackermann, *Opt. Continuum.* **2020**, *3*, 2036.
[24] W. N. Martens, R. L. Frost, J. Kristof, J. T. Kloprogge, *J. Raman Spectrosc.* **2002**, *33*, 84.
[25] John Wiley Sons, Inc. SpectraBase. **2024**. https://spectrabase.com
[26] A. Picard, I. Daniel, G. Montagnac, P. Oger, *Extremophiles* **2007**, *11*, 445.
[27] Y. Yu, Y. Wang, K. Lin, N. Hu, X. Zhou, S. Liu, *J. Phys. Chem. A* **2013**, *117*, 4377.
[28] G. Zhu, X. Zhu, Q. Fan, X. Wan, *Spectrochim. Acta A* **2011**, *78*, 1187.
[29] Y. S. Mary, L. Ushakumari, B. Harikumar, H. T. Varghese, C. Y. Panicker, *J. Iran. Chem. Soc.* **2009**, *6*, 138.
[30] A. R. Guerrero, R. F. Aroca, *J. Raman Spectrosc.* **2011**, *43*, 478.
[31] J. J. Cárcamo, A. E. Aliaga, E. Clavijo, C. Garrido, J. S. Gómez-Jeria, M. M. Campos-Vallette, *J. Raman Spectrosc.* **2011**, *43*, 750.
[32] M. Smith, A. G. Walton, J. L. Koenig, *Biopolymers* **2004**, *8*, 173.
[33] S.-H. Park, Y.-G. Kim, D.-H. Kim, H.-D. Cheong, W.-S. Choi, J.-I. Lee, *J. Opt. Soc. Korea* **2010**, *14*, 209.
[34] A. Vogel, J. Noack, K. Nahen, D. Theisen, S. Busch, U. Parlitz, D. X. Hammer, G. D. Noojin, B. A. Rockwell, R. Birngruber, *Appl. Phys. B: Lasers Opt.* **1999**, *68*, 271.
[35] A. Selvarajan, *Proc. Indian Acad. Sci.* **1966**, *64*, 44.
[36] T. Meyer, R. Ackermann, R. Kammel, M. Schmitt, S. Nolte, A. Tünnermann, J. Popp, *Analyst* **2019**, *144*, 7310.

How to cite this article: T. Koch, R. Ackermann, A. Stoecker, T. Meyer-Zedler, T. Gabler, T. Lippoldt, J. Missbach-Guentner, C. Russmann, J. Popp, S. Nolte, *J. Biophotonics* **2024**, *17*(9), e202300505. https://doi.org/10.1002/jbio.202300505